Langmuir

ARTICLE

pubs.acs.org/Langmuir

Study of Ionic Liquid Immobilization on Polyvinyl Ferrocene Substrates for Gas Sensor Arrays

Kuang-Yu Hou, Abdul Rehman, and Xiangqun Zeng*

The Department of Chemistry, Oakland University, Rochester, Michigan 48309, United States

Supporting Information

ABSTRACT: In this report, the effects of conductive polymer oxidation states and structures on the design and development of ionic liquid (IL)/conductive polymer (CP) composite films for gas sensing are systematically characterized. Four different polyvinyl ferrocene (PVF) films synthesized by varying the conditioning potential (0.7 vs 0.0 V) and the electrolyte are tested for their gas-sensing properties (e.g., sensitivity, selectivity, response time, linearity, and dynamic range against various gas analytes such as dichloromethane, ethanol, natural gas, methane, formaldehyde (37%), and benzene) utilizing the quartz crystal microbalance (QCM) and ATR-FT-IR. The best available film is further studied as a substrate for the immobilization of various ILs that enhanced both the sensitivity and selectivity. Finally, two arrays, each comprising four sensors with the following scheme are developed and characterized for their ability to classify the four target analytes by using linear discriminant analysis: (1) the highest sensitivity PVF film immobilized with four different ILs and (2) the highest sensitivity IL immobilized in four different PVF films. Array 2 is proven to be much better than array 1 in discriminating the analytes, which is very significant in establishing the fact that a diverse set of PVF redox states allow the rational development of a PVF/IL composite-based sensor array in order to analyze complex mixtures utilizing structural differences and the extent of intermolecular interactions.

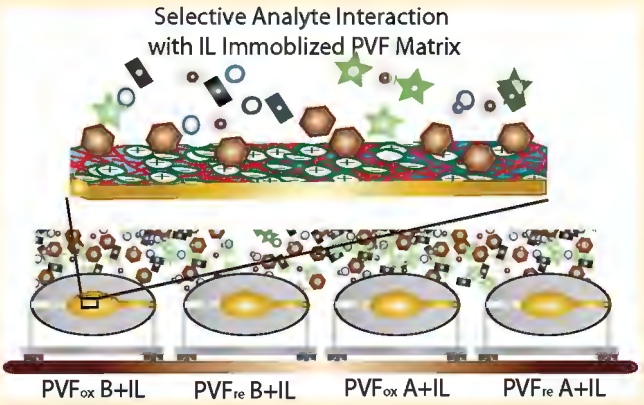

INTRODUCTION

Room-temperature ionic liquids (ILs) (also called low temperature molten salts) have attracted significant interest in the past few decades because of their unique chemical and physical properties. Owing to their negligible vapor pressure, remarkable thermal stability, and a wide liquid temperature range from as low as −96 °C to as high as 400 °C, they have been used as solvents in various organic,[1] inorganic, and polymeric materials as well as in analytical processes.[2] Their relatively low cost, ease of preparation, and potential to be reused and recycled make ionic liquids promising as potential green, eco-friendly media for many industrial and chemical applications. We and others have demonstrated that ILs are excellent materials for gas sensing[1,3−7] using a quartz crystal microbalance (QCM) and/or an electrochemical readout. Compared with organic gas-sensing materials, ILs are more stable and have a high solvation capacity for many volatile organic compounds and common gaseous analytes. Moreover, their synthetic flexibility enables ILs to be designed with the desired chemical properties. For example, the appropriate modification of the cation and anion can provide suitable functionality and allows much specific interaction between the target gas analyte and an individual IL. Therefore, the study, design, and development of ILs with functional and structural diversity to enhance chemical selectivity for the classification and identification of the gaseous analytes have been a major focus in our laboratory.

The development of IL-based gas sensors often requires the immobilization of ionic liquids on solid supports. An innovative method developed in our laboratory is to immobilize ILs on conductive polymer (CP) substrates so as to make IL/polymer composite films that can significantly enhance the sensitivity, specificity, and stability of IL-based gas sensors.[8] A CP is an organic polymer that can be transformed to a conductive form via oxidation or reduction of the nonconductive form of the polymer. The process of transforming a polymer to its conductive form is also called doping. By regulating the doping level, a conductivity between that of the undoped (insulating or semiconducting) and that of the fully doped (metallic) form of the polymer can be easily generated. CPs have been studied extensively as sensing materials for chemical sensors and sensor arrays because of the wide range of structural forms that can be synthesized and the ease by which changes can be made in the structure mechanically.[9−16] The adsorption of gas analytes at conductive polymers includes many nonbonding intermolecular

Received: October 18, 2010
Revised: February 17, 2011
Published: March 16, 2011

Table 1. Formula and Molecular Weight of ILs

Name	Formula	M.W. (g/mole)
$P_{666,14}PrSO_3$	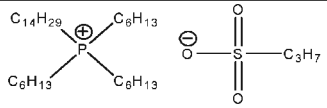	607.01
$P_{666,14}MS$	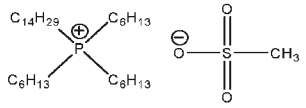	578.95
$P_{6666}CS$	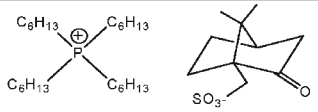	591.04
BmiCS	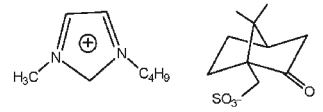	359.57

interactions such as dipole−dipole, van der Waals, hydrogen bonding, and $\pi-\pi$ complexes. These interactions can provide the chemical selectivity that is determined by the structure and properties of the conductive polymer and the analyte. It was reported that conducting polymers have a salt structure when prepared by the (electro)chemical oxidation or reduction of neutral precursors. The salt structure consists of two sublattices, one of which is formed from segments of the polymer chain carrying a positive or negative charge. The other sublattice is formed by (doped) counterions that maintain the overall electrical neutrality of the system. Changes in conductive polymer properties are linked to changes in the doped counterion's sublattice and polymer structures.[13,17] We intend to investigate here how various conductive polymer oxidation states affect their gas-sensing properties. Furthermore, we intend to provide a generic method for the development of ionic liquid-based gas sensors by understanding what oxidation state of the conductive polymer is the best substrate for subsequent ionic liquid immobilization and hence can be used to develop a novel strategy to look for highly robust and selectively responding sensing composites for high-tech sensing protocols.

The changes in the physical and chemical properties of the sensing materials can be transduced to current, absorbance, mass, or acoustic signals when they are exposed to the analytes. In this work, QCM and ATR-FT-IR techniques were used to characterize the conductive polymer and/or IL sensing material properties. Polyvinyl ferrocene (PVF) was selected as the model conductive polymer because the structure and properties of PVF can be altered through chemical or electrochemical oxidation and reduction and PVF can be easily made into a thin film. PVF is a positively charged polymer (Fc^+) in its oxidation state and neutral (Fc^0) in its reduction state. In this report, we systematically studied PVF films at two different oxidation states with two different structures and characterized their gas-sensing properties with different analytes. The optimum PVF film was used as a substrate for ionic liquid immobilization. The QCM sensor array using four different PVF films as well as PVF composite films with immobilized ILs ($P_{666,14}PrSO_3$, $P_{666,14}MS$, $P_{6666}CS$, and BmiCS; the structures are given in Table 1) were characterized for the analysis of dichloromethane,

Scheme 1. Illustration of IL Immobilization on PVF Substrates

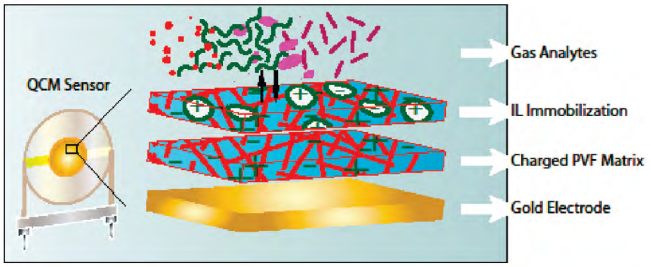

ethanol, natural gas, methane, formaldehyde (37%), and benzene over the range of concentration from 1 to 10% at room temperature (Scheme 1). It is foreseen that the completion of this project will allow new designs and the employment of this kind of conjugate as sensing materials that not only can analyze various analytes with industrial and health concerns but also can distinguish between analytes in the same organic class (e.g., different alcohols) in the form of arrays combined with pattern-recognition algorithms.

EXPERIMENTAL SECTION

Reagents. PVF was obtained from Polysciences, Inc. with an average MW of 25 000. Tetrabutylammonium perchlorate (TBAP) was purchased from GFS Chemicals, and sodium perchlorate (98%) was purchased from Sigma. Dichloromethane (ACS reagent grade, >99.5%) was purchased from Sigma-Aldrich. Benzene (ACS reagent grade) was obtained from Acros Organics, formaldehyde solution (37%) was obtained from GFS Chemicals, and denatured ethanol (reagent grade) was purchased from Aldrich. The saturated vapor pressure at room temperature is 100.84 mmHg for benzene, ca. 400.0 mmHg for dichloromethane, 24.5 mmHg for formaldehyde (37%), and 59.02 mmHg for ethanol. These reagents were used as received. Deionized water was purified using a Milli-Q water system (18 MΩ). Methane compressed gas (ultra-high-purity grade, >99.99%) was obtained from Praxair, Inc. Natural gas was used from a gas dispenser in the laboratory hood supplied by www.consumersenergy.com. It typically contains the following gases in the given mole % ranges: methane (90−96%), ethane (2.0−5.0%), propane (0.50−1.50%), *I*-butane (0.04−0.25%), *N*-butane (0.05−0.25%), *I*-pentane (0.01−0.03%), hexane (0.005−0.15%), CO_2 (0.50−1.5%), and nitrogen (0.50−2.0%).

ILs used in this study, including butylmethylimidazolium camphorsulfonate (BmiCS), tetrahexylphosphonium camphorsulfonate ($P_{6666}CS$), trihexyltetradecylphosphonium methanesulfonate ($P_{666,14}MS$), and tetradecyl-tri-*n*-hexylphosphonium propanesulfonate ($P_{14,666}PrSO_3$), have been synthesized by Dr. Rex Ren, IL-TECH Inc. (Middletown, CT) with over 98% purity following previous procedures.[18] The structures and formula weights of these ionic liquids are listed in Table 1, and their IR spectra as obtained by ATR-FT-IR are shown in the Supporting Information.

Instrumental Setup. Scheme 2 shows the instrumental setup for the characterization of the gas-sensing properties of the PVF and PVF/IL composite films. When analytes were gaseous samples (e.g., methane and natural gas), the sample gas cylinder was connected directly to a mass-flow controller (with a gas flow range of up to 100 SCCM, MKS Instruments Inc.). The N_2 carrier gas (compressed, Praxair, Inc.) is directly connected to a mass-flow controller (with a gas flow range of up to 500 SCCM) that was used to dilute and control the concentration of analytes. In this case, valves 1 and 3 are turned on while valves 2, 4,

dx.doi.org/10.1021/la104191n |*Langmuir* 2011, 27, 5136–5146

Scheme 2. Illustration of the Sensor Testing System via QCM or ATR-FT-IR

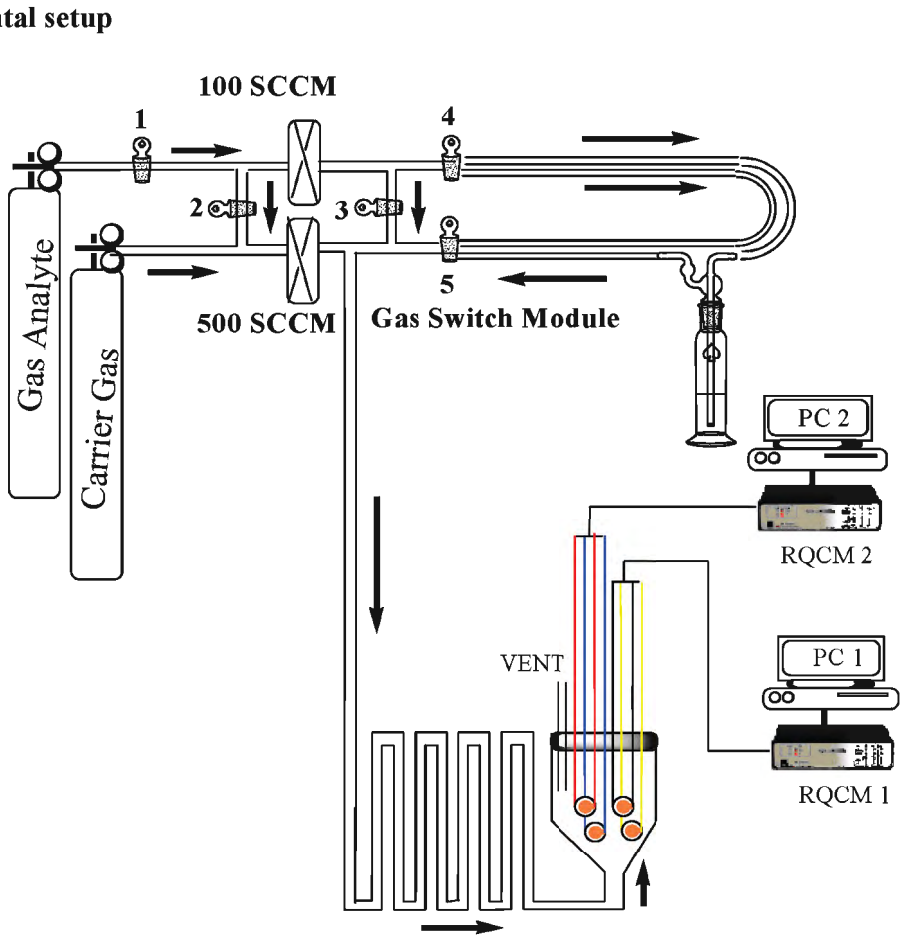

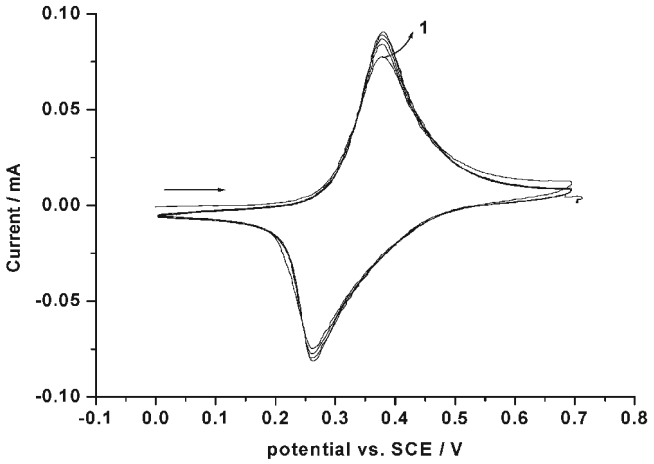

Figure 1. Cyclic voltammogram of a PVF-modified Au QCM electrode in a 0.1 M $NaClO_4$ solution.

and 5 are turned off. The analyte gas and nitrogen carrier gas flowed through glass coiled tubing to allow thorough mixing before reaching the gas sensor chamber in which the QCM sensors were mounted. The real-time readout data was recorded using two RQCMs (Maxtek, Inc.).

When the analytes are volatile organic compounds (VOC), valves 1 and 3 are shut off and valves 2, 4, and 5 are opened to allow the N_2 carrier gas to flow through a wash bottle filled with the liquid of the VOC to generate the vapor of the VOC. A fully saturated VOC stream is then further mixed with another N_2 carrier gas stream so as to obtain the required final concentration.

Characterization of PVF-Modified Electrodes. *PVF Film Preparation.* Commercial PVF was hydrophobic because it was synthesized with a final reduced state. The Au QCM electrode was coated with the PVF film via the electrochemical oxidation of PVF in 0.1 M TBAP with dichloromethane as the solvent. At the oxidative potential, PVF will have a positive charge and ClO_4^- in the electrolyte from TBAP will be doped into the PVF film as the counterions to maintain electroneutrality. Oxidized PVF is not soluble in dichloromethane and will precipitate from the dichloromethane solution and coat the electrode. The working electrode potential was stepped from 0.0 to 0.7 V repeatedly three times with a 3 min interval at each potential. After the QCM electrode was coated with the PVF film, the electrode was rinsed with deionized water and dried in N_2.

Preparation of PVF Films in Various Redox States. The redox property of a PVF-coated Au electrode was characterized by cyclic voltammetry (CV) in a 0.1 M $NaClO_4$ solution as shown in Figure 1. The oxidation peak (ca. 0.379 V) and reduction peak (ca. 0.264 V) were observed with a peak potential separation of about 115 mV. This is consistent with previous work in which the redox process of PVF is

dx.doi.org/10.1021/la104191n |*Langmuir* 2011, 27, 5136–5146

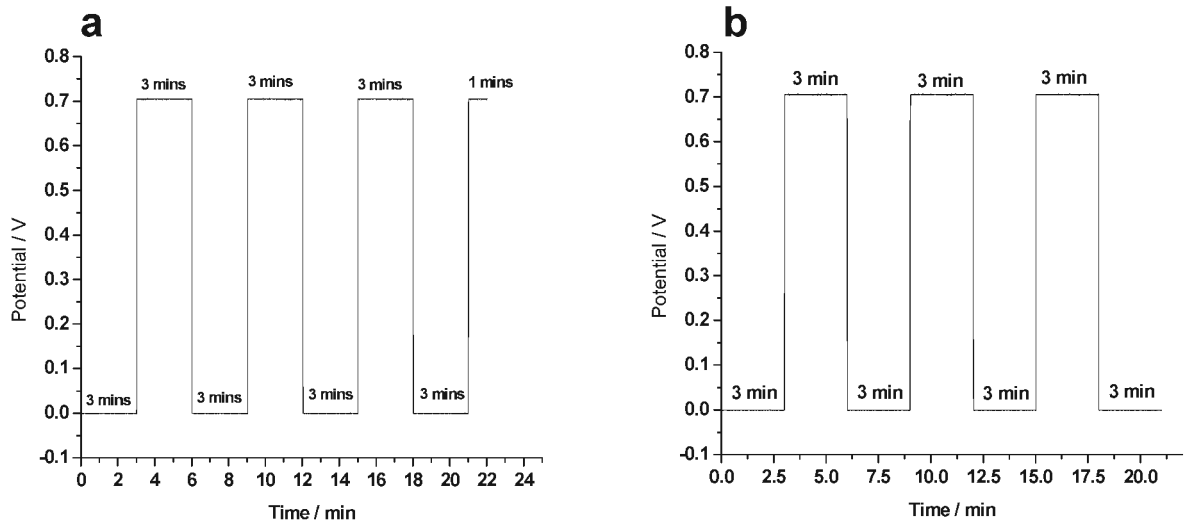

Figure 2. Conditioned potential step processes of PVF to form (a) oxidation ($PVF_{ox}A$) and (b) reduction ($PVF_{re}A$) states.

shown to be a one-electron transfer process (eq 1).

$$PVF^{+} \rightleftharpoons PVF + e^{-} \quad (1)$$

The current in the first cycle is lower than that in the following cycles, which is due to the well-known break in effects.[19]

The PVF-modified electrodes in different oxidation states were made by controlling the electrode potential in either an organic or aqueous solvent. $PVF_{ox}A$ and $PVF_{red}A$ films were made in 0.1 M TBAP in dichloromethane. A $PVF_{ox}A$ film was made when the potential was stepped up to 0.7 V for an additional 1 min at the end of the last oxidation step as shown in Figure 2a. The working electrode and the auxiliary electrode were immediately disconnected from the potentiostat. This prevents any newly formed PVF film from dissolving into the solvent. In contrast, a $PVF_{red}A$ film was made when the potential was stepped to 0.0 V for an additional 1 min at the end of the last reduction step as shown in Figure 2b. Finally, the PVF-modified electrodes were removed from the CH_2Cl_2, washed to remove additional PVF residues from the electrodes, rinsed with deionized water, and dried in N_2. Then electrodes were exposed to air for at least 45 min before their use in further experiments.

The $PVF_{ox}A$ and $PVF_{re}A$ QCM electrodes are further modified to form oxidation ($PVF_{ox}B$) and reduction ($PVF_{re}B$) states of PVF by the electrochemical redox cycling of $PVF_{ox}A$ and $PVF_{re}A$ in 0.1 M $NaClO_4$ solution between 0.0 to 0.7 V at a scan rate of 50 mV/s for five cycles. The post-treatment allows the reconfiguration of $PVF_{ox}A$ and $PVF_{re}A$ film structures in aqueous solvent, which are completely different from those formed in the organic solvent in which $PVF_{ox}A$ and $PVF_{re}A$ were made. The $PVF_{ox}B$ film was formed when the final CV potential was stopped at 0.7 V for an additional 1 min at the end of the last cycle as shown in Figure 3a. Then the electrodes were disconnected from the potentiostat. On the contrary, $PVF_{re}B$ was formed when the potential was stopped at 0.0 V for an additional 1 min at the end of the last cycle as shown in Figure 3b. Then the electrodes were further washed out with deionized water and dried in N_2. Finally, the electrodes were placed in a dark cabinet and dried thoroughly overnight.

The thickness of each (PVF/IL)-modified working transducer is different and measured by an Agilent Network impedance analyzer (Aligent Technologies, Inc., Santa Clara, CA). PVF redox state QCM sensor responses in terms of frequency change are normalized to the thickness of the PVF films (in $\mu g/cm^2$). The coverage range of PVF on QCM electrodes is from ca. 90 to 400 $\mu g/cm^2$, where $PVF_{ox}A$ is at ca. 96.4 $\mu g/cm^2$, $PVF_{ox}B$ is at ca. 367.5 $\mu g/cm^2$, and $PVF_{re}A$ is at ca. 292.9 $\mu g/cm^2$.

Immobilization of ILs onto PVF-Modified QCM Electrodes. Soaking methods were used to immobilize ionic liquids on the PVF-modified electrodes. IL ethanol solutions (0.1 M) were used.[20] The PVF electrodes were immersed overnight in a small cap containing 1 mL of diluted IL solution. Then the electrodes were dried in N_2 without any further rinsing and placed in a dark closet or drawer for an additional night to allow the solvent to evaporate. Layer thicknesses were measured with an LSE Stokes ellipsometer (model 7109-C370), and the density of these materials can be estimated by dividing the calculated mass per unit area by these thicknesses.

ATR-FT-IR Measurements. The FT-IR spectrometer experimental setup for our research is shown in Scheme 3. The ATR accessory (Specac Inc., Woodstock, GA) was operated with an Excalibur 3100 FT-IR from Varian, Inc. A transparent rectangular chamber is placed tightly in a flat zinc selenide prism (ZnSe, transmission range and IR range ca. 20 000−650 cm^{-1}) mounted on the top plate. The sample gas can flow in with the carrier gas and can leave through another exit where it is connected to the vent. FT-IR data was recorded at a resolution of 4 cm^{-1}.

DATA ANALYSIS

Sensor array data was analyzed using linear discriminant analysis (LDA). LDA is a means to attempt optimal class separation and seek the best class discriminatory information up to the highest possible accuracy from a group of different variables. LDA easily maximizes the ratio of intraclass variance while minimizing the interclass variance for data classification, which will help in accurately classifying objects into groups according to the dependencies and connections among variables. The frequency response of each sample gas at different concentrations from the sensing array was converted to a canonical variance from multidimensional space into 2D coefficients so that the distance can be calculated in multivariables and can classify the distributions of different sample gases. Discriminant analysis is used to find a linear combination of the measurements that best classify or discriminate among the gas analytes. The first two factor outcomes are the best discriminators in the group after a linear combination calculation of the gas analytes by the LDA. In the canonical variable plot, the data plots aggregate within groups of the same sample gas as a cluster. Otherwise, the data

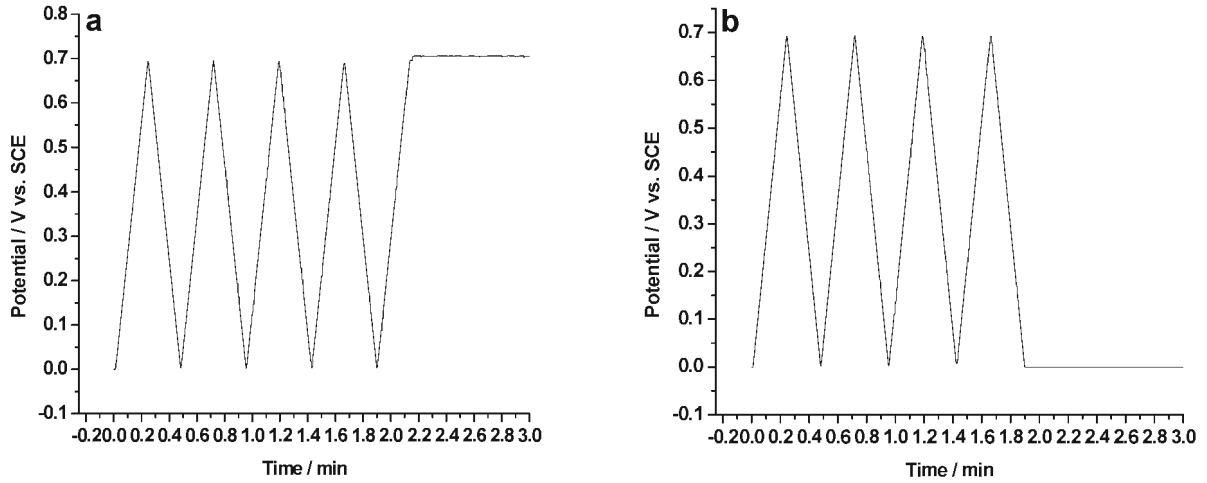

Figure 3. Potential step after the treatment of $PVF_{ox}A$ and $PVF_{re}A$ in $NaClO_4$ solution to form (a) oxidation ($PVF_{ox}B$) and (b) reduction ($PVF_{re}B$) states.

Scheme 3. ATR-FT-IR Setup for the Sample Gas Flow Cell System

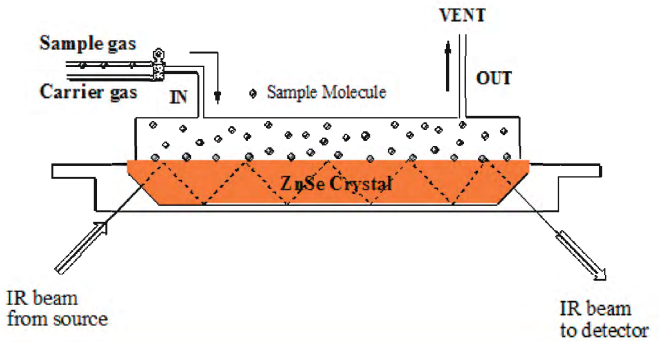

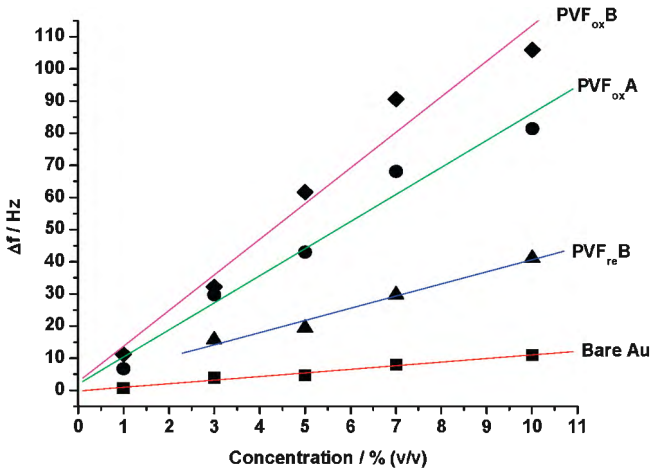

Figure 4. Δf as a function of the concentration of benzene vapor.

plots might separate into groups of different sample gases. If the pattern matrices can be 100% recognized from the LDA calculation, then the classification and identification of gas analytes by pattern recognition can be achieved with an optimal discriminative performance. LDA is generally more useful than PCA in our system because it is used to transform the data set into a more

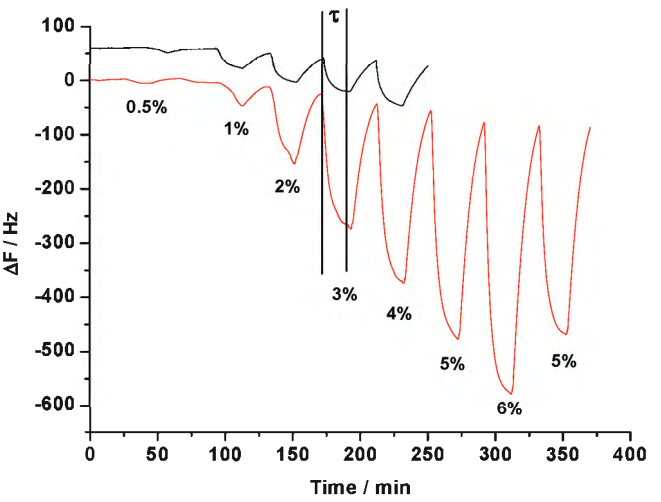

Figure 5. Frequency response of $PVF_{ox}B$ (black line) and $PVF_{ox}B$/BmiCS (red line) composite QCM sensors to different concentrations of benzene at room temperature.

easily controlled 2D plot and it is a self-consistent method that is able to produce greater differentiation and less overlap between groups. Therefore, other statistical algorithms are not demanded for our sensing system. In our case, commercial SYSTAT12 (Systat Software, Inc., Chicago, IL) statistics software was employed to perform the classification of different gas analytes.

RESULTS AND DISCUSSION

Effect of PVF Oxidation States on Gas Analyte Adsorption. The results of frequency changes as a function of analyte (benzene) concentration at $PVF_{ox}A$, $PVF_{ox}B$, $PVF_{re}A$, and a bare Au QCM electrode are summarized in Figure 4. $PVF_{re}B$ shows the least sensitivity for the gas analytes tested and was not included in the array testing. The calibration curves show that each sensor responds proportionally to the concentration of benzene over the range of concentration from 1 to 10% at room temperature. The different slopes in Figure 4 show that PVF in various oxidation states can provide chemical selectivity for gas

dx.doi.org/10.1021/la104191n |*Langmuir* 2011, 27, 5136–5146

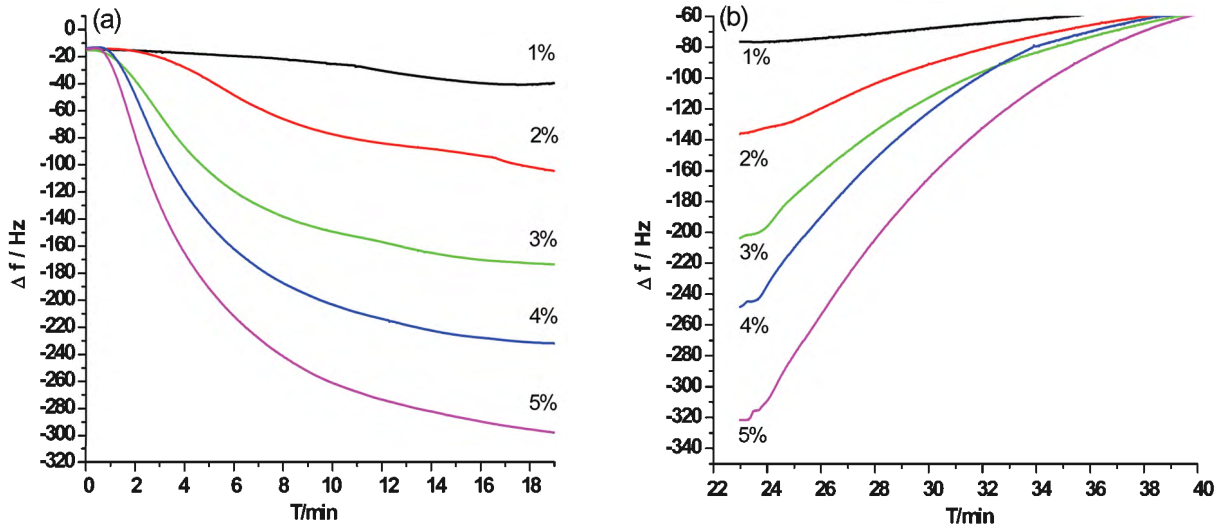

Figure 6. Sensing curves showing (a) adsorption and (b) desorption kinetics of the solvation process (~90% of response and recovery is achieved in 20 min). Note that these curves are parts of Figure 5 and the drift seen in the actual response is removed in this Figure, which shows that the real sensitivity is a bit less than what is shown in Figure 5.

analytes. $PVF_{ox}B$ has the highest slope and the highest sensitivity. It is likely that the process of $PVF_{ox}B$ film formation (i.e., conditioned by redox recycling in 0.1 M $NaClO_4$ and doped with ClO_4^-) promotes PVF film reconfiguration to have more surface area and a better structure, thus facilitating the adsorption of the target analytes. Figure 5 shows a representative QCM sensorgram of a $PVF_{ox}B$ and $PVF_{ox}B$/BmiCS composite film when they were repeatedly exposed to benzene vapor at various concentrations. The QCM sensor with the $PVF_{ox}B$/BmiCS film has a larger responses to the gas analyte than does the $PVF_{ox}B$ film alone. The ($PVF_{ox}B$/BmiCS)-coated QCM sensor exhibits a higher sensitivity to the adsorption and desorption of benzene than that without IL immobilization. Similar higher sensitivities were observed for the other PVF/IL composite films compared to the PVF films alone when they were exposed to various tested gas analytes (data not shown here). These results are consistent with our previous study that showed that CP substrates provide a greater surface area for thin IL film immobilization, which enables a higher sensitivity of IL-based gas sensors.[8,20] It is important to mention here that the response of the sensors with IL immobilization is a bit sluggish, which can be attributed to the porosity of the polymer films. When the pores are completely filled via immobilized ILs, the solvation and desolvation phenomena are slower than in the case in which the pores are empty, permitting quick transportation of the analytes in and out of the matrix.

Kinetics of Adsorption−Desorption Processes. The kinetics of adsorption and desorption phenomena can be explained by Figure 6. The response curve indicates that the gas sorption by the PVF film began immediately after the sample vapor was introduced into the sensor chamber. The rate of frequency shift is higher at the start and slows down with time. This can be connected to the equilibration of the adsorption−desorption process as well as the dynamic behavior of the gaseous interactions usually associated with this type of sensor system. The adsorption and desorption of molecules is a reversible reaction, so at the start, the velocity of molecules being solvated into the film is higher than that of the ones being solvated out of the film. As the process continues, the system tends to attain equilibrium where a steady state is achieved. Specific to the proposed strategy, after about 10 min, the sensing films have already achieved a saturation of 80−90%, which is enough for two reasons. First, the rate of further reaction is too slow to achieve absolute steady states because of time constraints usually observed in real life processes requiring high throughput. Second, because the pattern recognition would be a comparison protocol, strict obedience of the signal calculation over a specified time interval will eradicate the need for an absolute steady-state signal. As far as the recovery of the signals is concerned, it is even slower than the response. This indicates that the solvation of the analytes is a bulk process, not only a surface process. CPs have a network of interlinked channels that are filled with ILs to incorporate target analytes. For calculation purposes, we waited at least 20 min for the recovery and then let the next analyte in. However, it is important to mention that 100% recovery can be achieved by flowing nitrogen across the sensors for about 1 h. The data shown in Figure 6 is for benzene, but it also follows the same trend for other analytes. For this specific project, the calibration curve point is picked up by the average frequency drift of the gas analyte. The average is obtained and calculated by the origin software analysis function.

ATR-FT-IR Spectroscopic Characterization of Analyte and PVF/IL Interactions. ATR-FT-IR was used to characterize the interaction of gas analytes with the PVF and PVF/IL composite films. The PVF in the reduced state was dissolved in CH_2Cl_2 and cast on the ATR-FT-IR ZnSe substrate. The spectrum of air was used as the background spectrum, and the background-corrected IR spectra of BmiCS, P_{6666}CS, $P_{666,14}$MS, and $P_{666,14}PrSO_3$ between 600 and 3500 cm^{-1} are shown in Figure S1. Table S1 summarizes the characteristic major peaks of the ILs on the ZnSe. Similarly, the spectra of four ILs immobilized on the PVF film between 600 and 3500 cm^{-1} are shown in Figure S2. The peaks shifts were observed when four different ILs were immobilized on the PVF film, indicating the specific bond interactions between a particular IL and PVF film. Here, we discussed the characteristic peaks of the PVF/BmiCS composite film upon exposure to four analyte vapors as shown in Figure 7 and summarized peak shifts in Table 2. The peak intensities when

dx.doi.org/10.1021/la104191n |*Langmuir* 2011, 27, 5136–5146

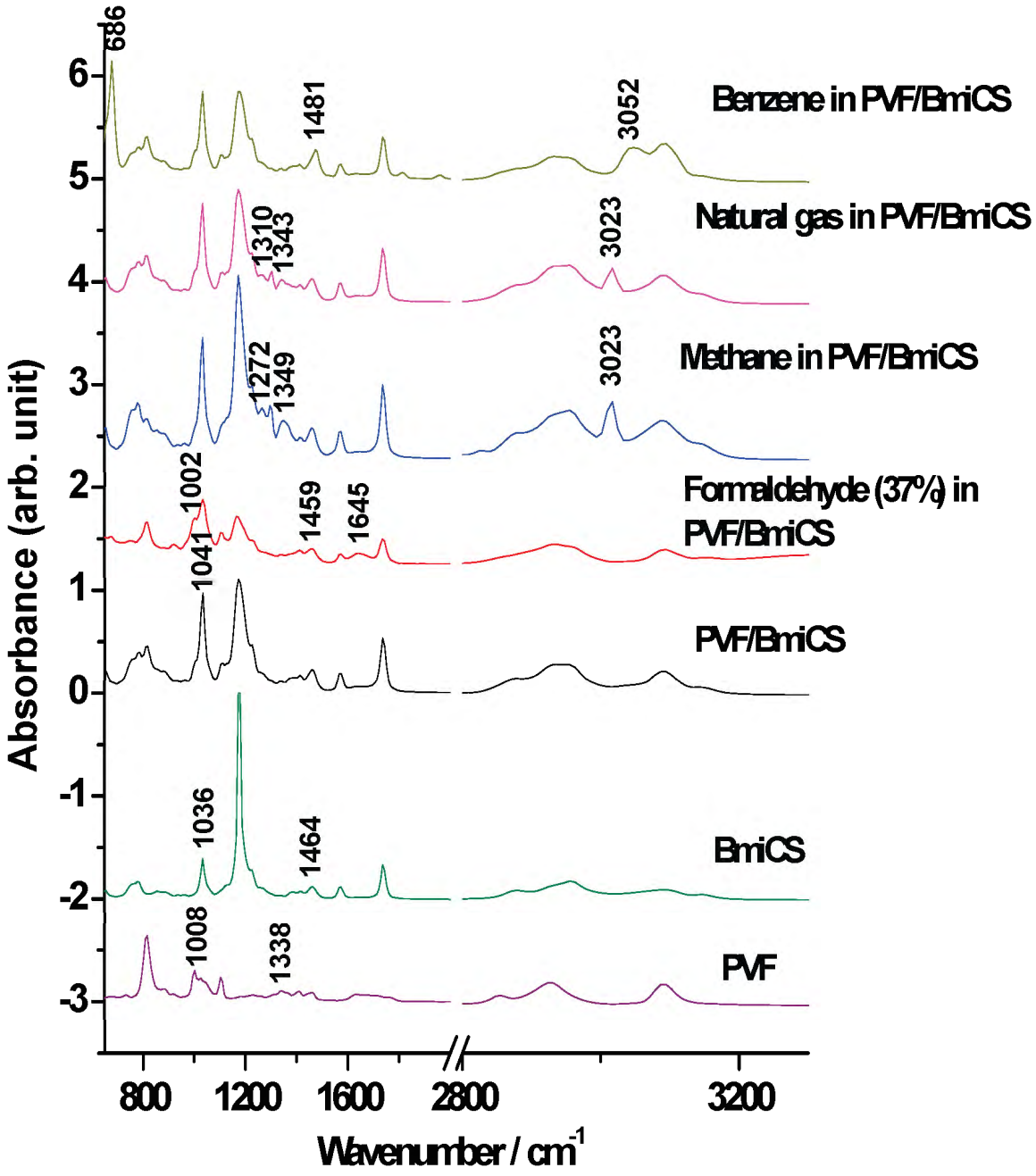

Figure 7. ATR-FT-IR spectra of PVF with BmiCS immobilization after the adsorption of benzene, natural gas, methane, formaldehyde (37%), the PVF/BmiCS film, BmiCS, and PVF.

Table 2. Summary of Characteristic Peak Shifts of Benzene, Natural Gas, Methane, Formaldehyde (37%), and PVF/BmiCS

	analyte gas major peak shifts compared to itself[a]	PVF/BmiCS peak shifts compared to PVF and BmiCS
benzene	Ar−H peak at 3047 cm^{-1} shifted to 3052 cm^{-1}; C−C peak at 1477 cm^{-1} shifted to 1481 cm^{-1}; C−H peak at 670 cm^{-1} shifted to 686 cm^{-1}	$-CH_2$ peak at 1464 cm^{-1} shifted to 1481 cm^{-1}
natural gas	C−H peak at 1303 cm^{-1} shifted to 1310 cm^{-1} and that at 3018 cm^{-1} shifted to 3023 cm^{-1}	$-CH_2$ peak at 1338 cm^{-1} shifted to 1343 cm^{-1}
methane	C−H peaks at 1262 cm^{-1} shifted to 1272 cm^{-1} and at 3018 cm^{-1} shifted to 3023 cm^{-1}	$-CH_2$ peak at 1338 cm^{-1} shifted to 1349 cm^{-1}
formaldehyde (37%)	$-CH_2$ peak at 1473 cm^{-1} shifted to 1459 cm^{-1}; >C═O peak at 1648 cm^{-1} shifted to 1645 cm^{-1}	$-CH_3$ peak at 1008 cm^{-1} shifted to 1002 cm^{-1}; $-SO_3^-$ peaks at 1036 cm^{-1} shifted to 1041 cm^{-1}

[a] See Figure S3.

dx.doi.org/10.1021/la104191n |*Langmuir* 2011, 27, 5136–5146

Table 3. Frequency Shifts of Modified Electrodes

electrode	F1	F2	F3	F4
	Different Amounts of $PVF_{ox}B$/IL Composites[a]			
QCM surface loading	$PVF_{ox}B$ + BmiCS	$PVF_{ox}B$ + $P_{6666}CS$	$PVF_{ox}B$ + $P_{666,14}PrSO_3$	$PVF_{ox}B$ + $P_{666,14}MS$
resonance frequency change (Hz)	86 400	66 200	40 200	52 800
layer thickness (nm)	413	227	183	199
calculated density ($\mu g/cm^3$)	9186	12 806	9645	11 653
electrode	H1	H2	H3	H4
	Different Amounts of PVF Redox State/BmiCS Composites[b]			
QCM surface loading	$PVF_{ox}A$ + BmiCS	$PVF_{ox}B$ + BmiCS	$PVF_{re}A$ + BmiCS	$PVF_{re}B$ + BmiCS
resonance frequency change (Hz)	39 600	53 200	48 300	52 600
layer thickness (nm)	164	179	209	223
calculated density ($\mu g/cm^3$)	10 164	13 050	9727	9928

[a] F1, $PVF_{ox}B$ + BmiCS, is ca. 379.4 $\mu g/cm^2$; F2, $PVF_{ox}B$ + $P_{6666}CS$, is ca. 290.7 $\mu g/cm^2$; F3, $PVF_{ox}B$ + $P_{666,14}PrSO_3$, is ca 176.5 $\mu g/cm^2$; and F4, $PVF_{ox}B$ + $P_{666,14}MS$, is ca. 231.9 $\mu g/cm^2$, as calculated from the frequency shifts. [b] H1, $PVF_{ox}A$ + BmiCS, is ca. 166.7 $\mu g/cm^2$; H2, $PVF_{ox}B$ + BmiCS, is ca. 233.6 $\mu g/cm^2$; H3, $PVF_{re}A$ + BmiCS, is ca. 203.3 $\mu g/cm^2$; and H4, $PVF_{re}B$ + BmiCS, is ca. 221.4 $\mu g/cm^2$, as calculated from the frequency shifts.

gas analytes were adsorbed on the PVF/BmiCS coating are several times higher than those on the PVF film only. The peak shifts observed when benzene, natural gas, methane, and formaldehyde (37%) are adsorbed onto ILs and PVF/IL composite films compared to Figures S1 and S2 indicate the specific bond interactions between a particular sample gas and ILs and PVF/IL composite films. The stronger the interaction of the gas analyte and the PVF/BmiCS composite, the larger the absorbance peak shift. For example, the $-SO_3^-$ group of BmiCS has two strong absorption peaks at 1036 and 1182 cm^{-1}. When formaldehyde (37%) is exposed, the $-SO_3^-$ group is shifted from 1036 to 1041 cm^{-1}. Both BmiCS and $P_{6666}CS$ have individual >C═O group major peaks at 1740 and 1734 cm^{-1}, and there is no change when they are compounded with the PVF polymer film. The sp^2- and sp-hybridized carbon atoms of PVF interact with >CH−, $-CH_2$, and $-CH_3$ functional groups that have overlap peaks between 2800 and 3200 cm^{-1} that are related to the imidazolium and phosphonium ions of ILs. There are no further peak shifts observed in the $-CH{=}CH_2$ out-of-plane bending and $-CH_2$ bending of PVF, indicating that these functional groups of PVF do not have any interaction with ILs. These results demonstrate the specificity of ILs and PVF/IL composites films for gas analyte detection and classification.

Gas Sensors with PVF and PVF/IL Composite Sensing Films. The ATR-FT-IR study supports the fact that the nonbonded intermolecular interactions (hydrogen bonding, $\pi-\pi$ stacking, dispersion forces, and long-range attractions) between each gas analyte and individual PVF or PVF/IL composite enable the partial selectivity of a sensor array to be built with these PVF and PVF/IL composite films. Below we show the gas-sensing properties of two arrays. In the first array, $PVF_{ox}B$ was used as the same substrate and four different ILs (BmiCS, $P_{6666}CS$, $P_{666,14}MS$, and $P_{666,14}PrSO_3$) were immobilized, and we intended to determine whether the selectivity of ILs is sufficient to classify the four target analytes. The $PVF_{ox}B$ was selected because it has the strongest interaction with the most gas analytes selected in this study. Film thicknesses after electrografting and immobilization of all of these sensors are provided in Table 3.

The frequency changes as a function of the concentration of the four analytes are shown in Figure S4. The calibration curves show that the $PVF_{ox}B$/BmiCS composite gives the highest signal for all four analytes. This may be due to the strong molecular dipole−induced dipole interaction between gas analytes and alkylbenzenesulfonate anions of BmiCS. Both methane and natural gas have very small responses and low selectivities to $PVF_{ox}B/P_{6666}CS$, $PVF_{ox}B/P_{666,14}MS$, and $PVF_{ox}B/P_{666,14}PrSO_3$ QCM sensors. In the second array, BmiCS was selected as the ionic liquid and it was immobilized on four PVF substrates with various charge states. Figure 8 shows the frequency change of PVF/BmiCS composite films upon exposure to each analyte at various concentrations. The calibration curves show that the selectivity of the PVF/BmiCS sensor array is much higher than that of the $PVF_{ox}B$/IL sensor array. This result is significant because it suggests that PVF in various charge states significantly affects the selectivity of the PVF/IL composite films. Here it is important to note that methane and natural gas demonstrate quite different responses, although a major part of natural gas is methane. This can be explained by the presence of highly polar components of natural gas in addition to methane, which can have a significant impact on QCM-based sensors; this is a very sensitive technique that is able to detect nanogram levels of change; however, ATR-FT-IR peak shifts due to the presence of these molecules in the stream mainly composed of methane might be very small to observe. Additionally, the mass sensors are the devices capable of detecting mass changes, so even the proportions of these polar compounds are much less than those of methane yet they can produce much larger effects because their mass is higher than that of methane for the same number of molecules. For example, hexane is present in natural gas and has a molar mass of 86.18 g/mol as compared to methane with a molar mass of 16.04. Thus, a molecule of hexane can produce an effect that is 5 times that of a molecule of methane. This is also true of other molecules present in natural gas.

One more contradiction is visible when we compare the results from the two arrays. Sensors F1 and H2 are built with the same composition of sensing material and differ from each other only with respect to the amount of material coated onto the surface of the QCM device. However, the responses shown are not exactly proportional to the amount of material. For that reason, we measured the thicknesses of all of the layers formed using ellipsometry and then calculated the density of the layers by dividing the amount of material by the measured thickness. This

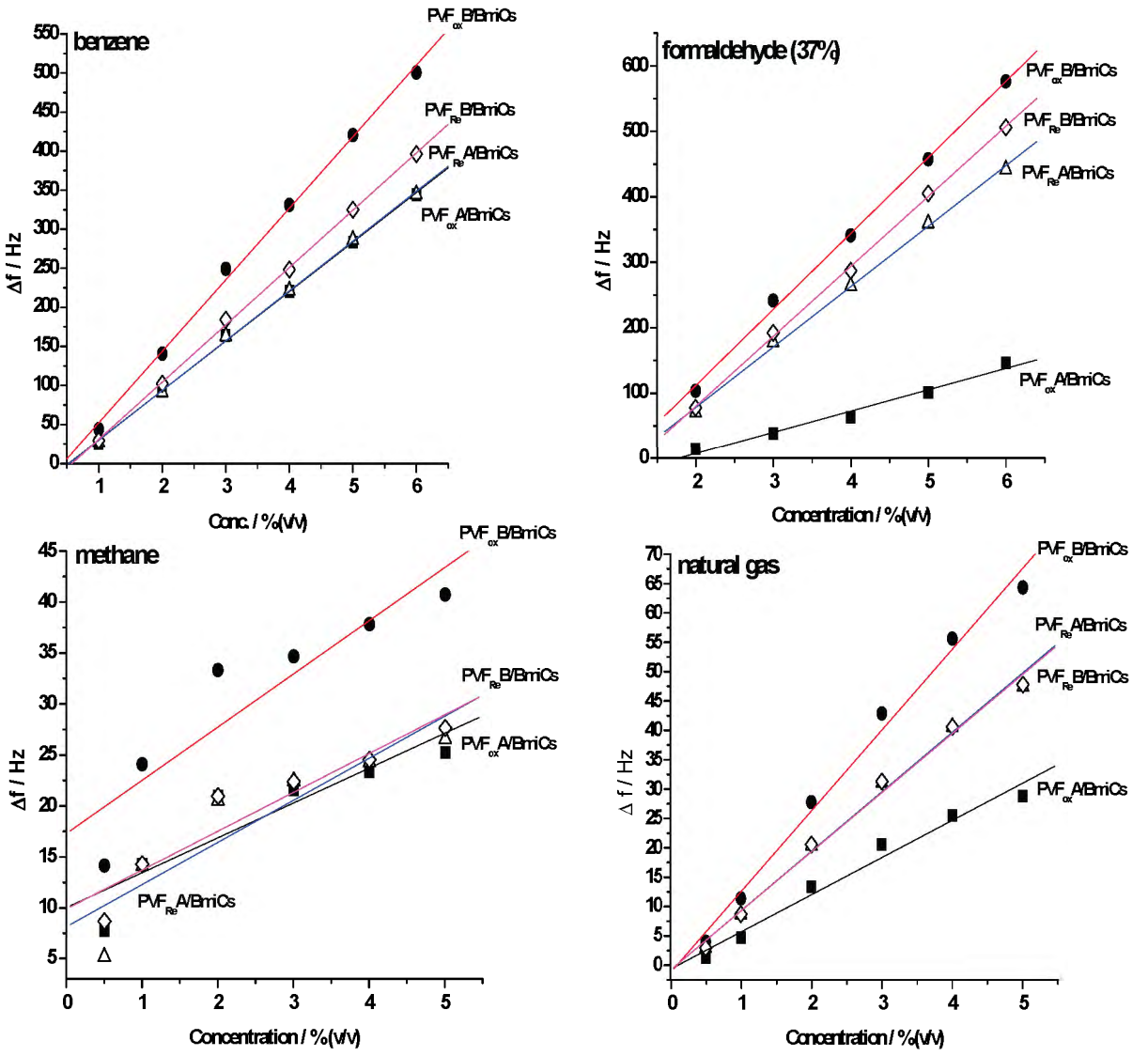

Figure 8. Δf as a function of the concentrations of four organic sample gases for benzene, formaldehyde (37%), methane, and natural gas for PVF redox states ($PVF_{ox}A$, $PVF_{ox}B$, $PVF_{re}A$, and $PVF_{re}B$) with BmiCS immobilization. The straight lines represent the linear fit to the data.

helped us to explain the sensor responses (i.e., if the density of the material is higher, then the porosity will be lower, which can contribute to lowering the sensitivity in two ways). First, the low porosity means a higher stacked polymer matrix, which can reduce the number of interactions that the analyte can produce with the sensor, and thus a lower effect, and this effect is greatly enhanced when the sensor is based on the bulk effect sensor material rather than the surface effect. Second, a higher density can reduce the number of interlinked transport channels inside the matrix, which are especially significant in our case. When we try to immobilize the IL inside the polymer, a higher resistance is faced by the IL when being distributed because of less channeling inside. The IL has to play a significant role in determining the sensor response, which is hindered by this low porosity. Because the porosity of sensor F1 is much higher than that of H2, it can produce a much larger effect for most of the analytes in proportion to the latter. Another factor that is influential with respect to the sensitivity of the polymer layers is the redox state of the polymer. When the polymers are synthesized through an electrochemical process, there is a movement of counterions in and out of the matrix with the cycling of oxidized and reduced states, respectively, before reaching a relaxed configuration. This movement is called doping and undoping, and the whole phenomenon is called the break-in effect, which depends upon the nature and concentration of the supporting electrolyte as well as the layer thickness. When PVF is in a doped state, it is more hydrophilic than when it is in an undoped state and in this particular case show higher responses because the interactions are mostly polar in nature. Therefore, different polarities of the films due to the variation in this phenomenon can produce some variable effects.

LDA was used to analyze these two arrays for pattern recognition of the selected analytes. The sensing signals were normalized by the surface loading of PVF, IL coating amount ($\mu g/cm^2$), and concentration of gas samples (100 g/m^3). Because the responses of the frequency shift with concentration change in various PVF/IL composite films having good linearity, it renders a good accuracy of the pattern identification and classification.

Four replicate data were selected from each gas analyte on the different PVF/IL composite films. The LDA result in Figure 9A

dx.doi.org/10.1021/la104191n |*Langmuir* 2011, 27, 5136–5146

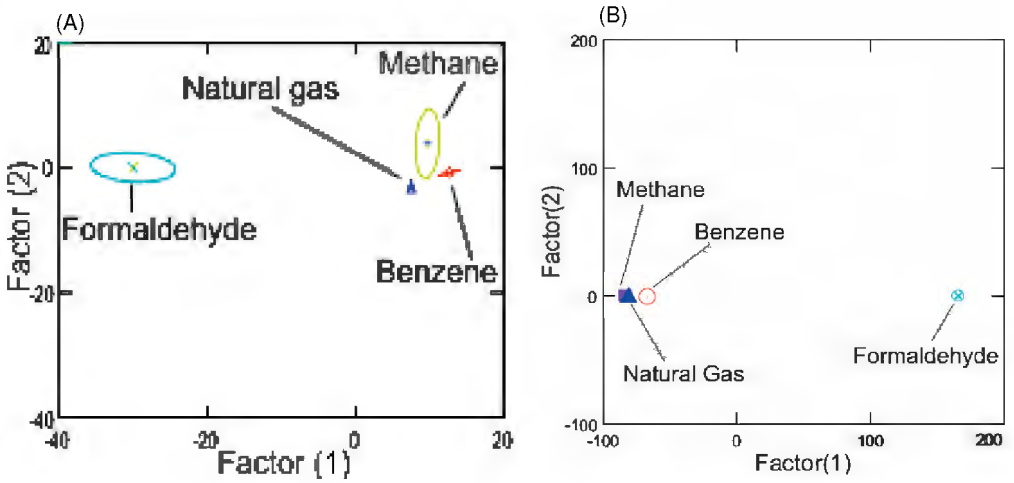

Figure 9. LDA canonical means plots of the four vapors tested against (A) PVF redox state coatings with a BmiCS immobilization sensor array by four replicate data sets and (B) $PVF_{ox}B$ with a four IL immobilization sensor array by five replicate data sets.

shows that the PVF/BmiCS array has a much higher classification accuracy compared to the $PVF_{ox}B$/IL array (shown in Figure 9B). There is no overlap of the mean group cluster for four gas analyte variances in the canonical means plot for the PVF/BmiCS array. The formaldehyde group (37%) is far away from other gas analyte groups because of the high polarity index of organic vapor and strong hydrogen bond interaction with the composite film. Methane and natural gas are very similar to each other but quite separate from benzene. The classification of benzene, formaldehyde (37%), and natural gas is correct, with 100% accuracy, whereas 75% accuracy was observed for methane as shown in the "jackknifed" classification matrix in Tables S2 and S3. The jackknifed analysis is able to correctly classify 15 out of 16 of the measured gas analytes with an overall accuracy rate of 94%. Considering the potential of available conductive polymers and ILs choices, a great sensor array can be designed and built for the pattern recognition of volatile gases in real world applications.

CONCLUSIONS

Four different PVF films with varied oxidation states are electrochemically synthesized by switching the conditioning potentials and electrolyte compositions and characterized for their sensing and discriminating abilities for a class of analytes with industrial and public importance. Results show that the properties of conducting polymer PVF such as redox states and post-treatment play significant roles in developing and defining their gas-sensing mechanisms. The PVF film made in an organic solvent that was conditioned by further redox cycling in 0.1 M $NaClO_4$ ($PVF_{ox}B$) gave the highest sensitivity for most analytes tested. This film was further explored by immobilizing different ILs into it, which enhanced the sensitivity from 2 to 5 times that of pure PVF films. Among the four ILs tested (BmiCS, $P_{6666}CS$, $P_{666,14}MS$, and $P_{666,14}PrSO_3$), the experimental data showed that $PVF_{ox}B$/BmiCS gave the highest sensitivities for all four gas analytes. The current detection limit for a gas analyte with a polarity index of >1 was as low as about 1% at room temperature. ATR-FT-IR analysis supported the observations from the QCM data in one way and also helped us to predict the directions of this work by describing the extent of interaction capabilities of the proposed films. Thus, a diverse set of PVF redox states and PVF/IL composites allowed us to develop two sensor arrays, each consisting of four channels, so as to generate the selective response of analyte mixtures resulting from structural differences and intermolecular interactions for pattern recognition. Using LDA, we were able to classify the analyte classes successfully with an accuracy of 94%. This opens up an exciting possibility to explore these conducting polymers and diversify their applications by viable immobilizations to build an assay for fast, reliable, highly sensitive, selective detection.

ASSOCIATED CONTENT

Supporting Information. ATR-FT-IR spectra of gas analytes, ILs, and PVF/ILs. IL characterization of the PVF/IL films for sensing by QCM. Signal pattern recognition of the results from PVFoxB/IL composites. This material is available free of charge via the Internet at http://pubs.acs.org.

AUTHOR INFORMATION

Corresponding Author
*E-mail: zeng@oakland.edu.

ACKNOWLEDGMENT

This research was supported in part by the NIOSH R21 (1R21Oh009099-01A1) and in part by an ONR grant (N000141010734). We thank Dr. Xiaofeng R. Ren for help with ionic liquid synthesis.

REFERENCES

(1) D'Anna, F.; Frenna, V.; Noto, R.; Pace, V.; Spinelli, D. Room temperature ionic liquids structure and its effect on the mononuclear rearrangement of heterocycles: an approach using thermodynamic parameters. *J. Org. Chem.* **2006**, *71*, 9637–9642.

(2) Yokozeki, A.; Shiflett, M. B. Hydrogen purification using room-temperature ionic liquids. *Appl. Energ.* **2007**, *84*, 351–361.

(3) Wang, R.; Hoyano, S.; Ohsaka, T. O_2 gas sensor using supported hydrophobic room-temperature ionic liquid membrane-coated electrode. *Chem. Lett.* **2004**, *33*, 6–7.

(4) Buzzeo, M. C.; Hardacre, C.; Compton, R. G. Use of room temperature ionic liquids in gas sensor design. *Anal. Chem.* **2004**, *76*, 4583–4588.
(5) Zhao, D.; Wu, M.; Kou, Y.; Min, E. Ionic liquids: applications in catalysis. *Catal. Today* **2002**, *74*, 157–189.
(6) Liang, C.; Yuan, C.-Y.; Warmack, R. J.; Barnes, C. E.; Dai, S. Ionic liquids: a new class of sensing materials for detection of organic vapors based on the use of a quartz crystal microbalance. *Anal. Chem.* **2002**, *74*, 2172–2176.
(7) Kenneth, R. S. Ionic liquids for clean technology. *J. Chem. Technol. Biotechnol.* **1997**, *68*, 351–356.
(8) Yu, L.; Jin, X.; Zeng, X. Methane interactions with polyaniline/butylmethylimidazolium camphorsulfonate ionic liquid composite. *Langmuir* **2008**, *24*, 11631–11636.
(9) Nguyen, A. L.; Luong, J. H. T. Mediated glucose biosensor based on polyvinylferrocene. *Appl. Biochem. Biotechnol.* **1993**, *43*, 117–132.
(10) Murray, R. W. *Techniques of Chemistry: Molecular Design of Electrode Surfaces*; John Wiley & Sons: New York, 1992.
(11) Wnag, X. B.; Bonnett, J. M.; Pethig, R.; Baker, P. A.; Parri, O. L.; Underhill, A. E. Electrochemical properties of substituted polyvinylferrocene films. *J. Mol. Electron.* **1991**, *7*, 167–178.
(12) Dong, S.; Che, G. Electrocatalysis at a microdisk electrode modified with a redox species. *J. Electroanal. Chem.* **1991**, *309*, 103–114.
(13) Kuzmany, H.; Mehring, M. *Electronic Properties of Polymers and Related Compounds*; Springer-Verlag: Berlin, 1989; p 18.
(14) Kannuck, R. M.; Bellama, J. M.; Blubaugh, E. A.; Durst, R. A. Cross-linked poly(vinylferrocene)-modified reference electrode for nonaqueous electrochemistry. *Anal. Chem.* **1987**, *59*, 1473–1475.
(15) Hillman, A. R. *Electrodechemical Technology of Polymers*; Elsevier: London, 1987.
(16) Seanor, D. A. *Electrical Properties of Polymers*; Academic Press: New York, 1982; p 6.
(17) Xie, L. K.; Buckley, L. J.; Josefowicz, J. Y. Observations of polyaniline surface-morphology modification during doping and dedoping using atomic-force microscopy. *J. Mater. Sci.* **1994**, *29*, 4200–4204.
(18) Ren, R. X.; Wu, J. X. Mild conversion of alcohols to alkyl halides using halide-based ionic liquids at room temperature. *Org. Lett.* **2001**, *3*, 3727–3728.
(19) Tang, Y.; Zeng, X. Poly(vinyl ferrocene) redox behavior in ionic liquids. *J. Electrochem. Soc.* **2008**, *155*, F82–F90.
(20) Jin, X.; Yu, L.; Zeng, X. Enhancing the sensitivity of ionic liquid sensors for methane detection with polyaniline template. *Sens. Actuators, B* **2008**, *133*, 526–532.